Available online at www.sciencedirect.com
SCIENCE DIRECT®
ELSEVIER
International Journal of Solids and Structures 43 (2006) 2904–2931
INTERNATIONAL JOURNAL OF SOLIDS and STRUCTURES
www.elsevier.com/locate/ijsolstr

Some recent developments on integrity assessment of pipes and elbows. Part I: Theoretical investigations

J. Chattopadhyay [a,*], H.S. Kushwaha [a], E. Roos [b]

[a] *Reactor Safety Division, Hall-7, Bhabha Atomic Research Centre, Mumbai 400085, India*
[b] *Material Testing Institute, MPA, Pfaffenwaldring 32, University of Stuttgart, D-70569 Stuttgart, Germany*

Received 28 January 2005; received in revised form 13 June 2005
Available online 18 August 2005

Abstract

Integrity assessment of piping components is very essential for safe and reliable operation of power plants. Over the last several decades, considerable work has been done throughout the world to develop a system oriented methodology for integrity assessment of pipes and elbows, mainly for application to nuclear power plants. However, there is a scope of further development/improvement of issues, particularly for pipe bends, that are important for accurate integrity assessment of pipings. Considering this aspect, a comprehensive *Component Integrity Test Program* was initiated in 1998 at Reactor Safety Division (RSD) of Bhabha Atomic Research Centre (BARC), India in collaboration with MPA, Stuttgart, Germany through Indo-German bilateral project. In this program, both theoretical and experimental investigations were undertaken to address various issues related to the integrity assessment of pipes and elbows. The important results of the program are presented in this two-part paper. In the part I of the paper, the theoretical investigations are discussed. Part II will cover the experimental investigations. The theoretical investigations considered the following issues: new plastic (collapse) moment equations of defect-free elbow under combined internal pressure and in-plane closing/opening moments; new plastic (collapse) moment equations of throughwall circumferentially cracked elbow, which are more accurate and closer to the test results; new 'η_{pl}' and 'γ' functions of pipes and elbows with various crack configurations under different loading conditions to evaluate J–R curve from test data; and the effect of deformation on the unloading compliance of TPB specimen and throughwall circumferentially cracked pipe to measure crack growth during fracture experiment. These developments would also help to study the effect of stress triaxiality in the transfer of material J–R curve from specimen to component.

Keywords: Pipe; Pipe bend; Crack; Integrity assessment; Limit load; J–R curve

* Corresponding author. Tel.: +91 22 25591522; fax: +91 22 25505151.
E-mail address: jchatt@apsara.barc.ernet.in (J. Chattopadhyay).

0020-7683/$ - see front matter © 2005 Elsevier Ltd. All rights reserved.
doi:10.1016/j.ijsolstr.2005.06.054

Nomenclature

a_0, a	initial, current crack length per crack tip for throughwall crack and crack depth for part-through crack
A	crack area
D, D_m	Outer, mean diameter of pipe/elbow cross section
E	Young's modulus
F_L	limit load
h	$= tR_b/R^2$, elbow factor or pipe bend characteristics
J, J_e, J_p	total, elastic, plastic J-integral
J_{app}	applied J-integral
$(J_i)_{SZW}$	J-initiation toughness from stretched zone width
M	total applied moment
M_L	limit moment (collectively used to define instability or plastic collapse moment)
m	$= M/M_L$, normalized moment
M_0	limit moment (collectively used to indicate instability or plastic collapse) for defect-free pipe/elbow
$m_0 = M_0/4R^2t\sigma_y$	normalized limit moment for defect-free pipe/elbow
P	total applied load
P_r	internal pressure
p	$= P_rR/t\sigma_y$, normalized internal pressure
R, R_i, R_o	mean, inside, outside radius of pipe/elbow cross section
R_b, R_{bi}, R_{bo}	bend radius of elbow at crown, intrados, extrados
s	$= \frac{T}{2\pi Rt\sigma_f}$ = normalized axial tension
t	wall thickness of pipe/elbow
T	axial tension in pipe
X	$= M_L/M_0$, weakening factor of throughwall circumferentially cracked elbow plastic (collapse) moment due to the presence of crack
x	$= a/t$ for part-through crack

Greek symbols

α	half axial crack angle in elbow
α_0	initial half axial crack angle in elbow
Δ_{pl}	plastic load-line displacement
ϕ_{pl}	plastic load-point rotation
γ	a function to correct the J-integral evaluated by 'η' factor in crack growth situation (Eq. (28))
η	a function to multiply the area under the load vs. load-point-deflection curve to get the J-integral
η_{pl}	a function to multiply the area under the load vs. plastic load-point-deflection curve to get the plastic component of the J-integral (Eq. (28))
λ	normalized unloading compliance
ν	Poisson's ratio
θ	half circumferential crack angle
σ_y	material yield stress
σ_f	material flow stress defined as the average of yield and ultimate strength
ζ	$= t/R_0$

Abbreviations

CMOD	crack mouth opening displacement
J–R	*J*–resistance
NB	nominal bore diameter
TCC	throughwall circumferentially cracked
TES	twice-elastic slope
TPB	three point bend

1. Introduction

Integrity assessment of piping components is very essential for safe and reliable operation of all types of process power plants. It is especially important for nuclear power plants because of the application of leak-before-break (LBB) concept which involves detailed integrity assessment of primary heat transport piping systems taking into account the postulated cracks. The mechanical evaluation of pipe failures has evolved over time. An initial purpose of such analysis was to determine the causes of large breaks occurring in oil and gas pipelines. The development of commercial nuclear power plants initiated the need for additional tools to assess the reliability and failure behavior of pressure vessel and piping components under different loading and environmental conditions. The results of these efforts have been transferred to other relevant industrial branches as well. The main effort in evaluating the mechanical and structural behavior of pressurized components started about 1950. Since that time, numerous investigations have been performed to assess the loading capacity and failure behavior of piping components. Investigations have also focused on determining failure loads and quantifying the margins of safety. While a considerable work has already been done in the development of integrity assessment procedure of cracked/un-cracked piping components, some issues are still unresolved or not fully understood, especially regarding elbows.

Against this backdrop, a comprehensive *Component Integrity Test Program* was initiated in 1998 at Bhabha Atomic Research Centre (BARC), India in collaboration with MPA, Stuttgart, Germany. In this program, both theoretical and experimental investigations were undertaken to address various issues related to the integrity assessment of pipes and elbows. The important results of the program are presented in this two-part paper. In this part I of the paper, the theoretical investigations are discussed. Part II (Chattopadhyay et al., 2005b) will cover the experimental investigations.

In the theoretical part, the following issues are addressed:

- New plastic (collapse) moment equations of defect-free elbows subjected to combined internal pressure and bending moment have been proposed. The existing equations are applicable for pure bending moment only, whereas the actual service condition is usually a combination of internal pressure and bending moment.
- New plastic (collapse) moment equations of throughwall circumferentially cracked elbows are proposed, which are more consistent and closer to the test results.
- New limit load based generalized expressions of 'η_{pl}' and 'γ' have been proposed to evaluate *J–R* curve from test results. The implication of these new basic equations is that for any new specimen geometry and loading condition for which limit load formula is available, specimen/component *J–R* curve can be obtained from test data. On this basis, new 'η_{pl}' and 'γ' functions for pipes and elbows with various crack configurations under different loading conditions have been derived.
- The effect of deformation, if any, on the unloading compliance correlation of commonly used ASTM SE(B) (also known as three point bend, TPB) specimens and cracked pipe has been investigated for

measurement of crack growth during fracture mechanics experiments. The existing equations do not consider this effect.

Each of these studies is described below briefly.

2. New limit load equations of defect-free elbow under combined internal pressure and in-plane bending moment

Pipe bends or elbows are commonly used components in a piping systems. It is important to know its limit load for the safe operation of the plant. The term '*limit load*' is used in this paper in a generic sense to collectively indicate either plastic instability or plastic (collapse) load. As per the definition of Gerdeen (1979), the *plastic instability load* is characterized by the zero slope of the load–deflection curve, which means the maximum load in the monotonic load–deflection curve (see Fig. 1). *Plastic* (*collapse*) *load* indicates a load where significant plastic deformation occurs, determined by applying a criterion of plastic collapse (e.g. twice-elastic slope (TES) as recommended by ASME (2000)) on the load–deflection curve. TES criterion is shown in Fig. 1. In this paper, plastic load has always been evaluated by TES criterion. Different studies had earlier been carried out and various equations were proposed to evaluate the limit load of elbows. They are mostly applicable for pure bending moment. However, in actual service condition, an elbow is usually subjected to combined internal pressure and bending moment. No limit moment equation is available which takes into account the effect of internal pressure. The present study attempts to address this issue and propose new limit moment equations of defect-free elbow under combined internal pressure and bending moment. More details of this work are available in Chattopadhyay et al. (2000) and Chattopadhyay (2002).

2.1. Background

Marcal (1967) was the first to present the results for elastic–plastic behavior of pipe bends with in-plane bending moment. Spence and Findlay (1973) found approximate bounds on limit moments for in-plane

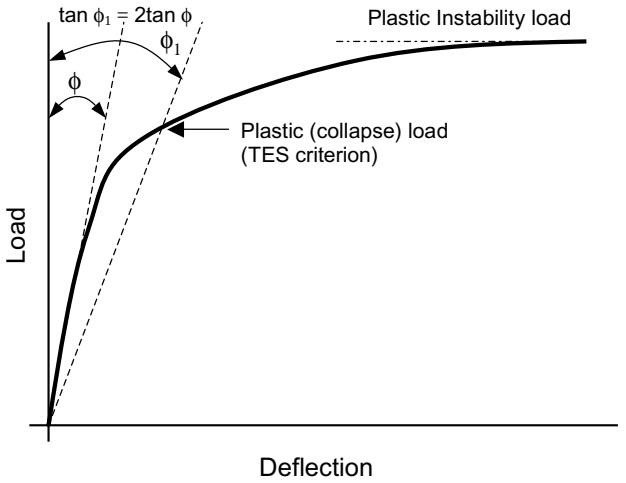

Fig. 1. Definitions of limit load.

bending by utilizing previously existing analyses in conjunction with the limit theorems of perfect plasticity. Spence and Findlay (1973) expressed the lower-bound in-plane limit moment of an elbow as

$$M_0 = 0.8h^{0.6}(D^2 t\sigma_y); \quad \text{for } h < 1.45$$
$$= (D^2 t\sigma_y); \quad \text{for } h > 1.45 \tag{1}$$
$$h = tR_b/R^2 \tag{2}$$

where h is the elbow factor or pipe bend characteristics, R_b is the mean bend radius of elbow, D is the outer diameter, R is the mean radius of elbow cross section and t is the wall thickness of elbow.

Calladine (1974) tried to find the lower-bound limit moment of a thin curved tube under pure bending moment by using the classical elastic shell analysis in conjunction with the limit theorems of plasticity. Calladine (1974) expressed the lower-bound in-plane plastic (collapse) moment as

$$M_0 = 0.935h^{2/3}(4R^2 t\sigma_y); \quad \text{for } h < 0.5 \tag{3}$$

Both the above expressions are based on small-displacement analysis and assume ideal plastic material behavior. Based on large displacement analysis Goodall (1978a) proposed the maximum load carrying capacity of the elbow subjected to closing bending moment as

$$M_0 = \frac{1.04h^{2/3}(D^2 t\sigma_y)}{(1+\beta)} \tag{4}$$

with,

$$\beta = \left(2 + \frac{(3h)^{2/3}}{3}\right)\left(\frac{4\sqrt{3(1-\nu^2)}}{\pi}\cdot\frac{\sigma_y}{E}\cdot\frac{R}{t}\right) \tag{5}$$

Griffiths (1979) performed experimental study on both cracked and un-cracked elbows mainly to see the effect of cracks on limit loads. For un-cracked elbow, he suggested to multiply the Calladine (1974) formula (Eq. (3)) by a factor of 1.33 to account for the stiffening effect of tangent pipes attached to the elbow. Touboul et al. (1989) proposed the following equations of plastic (collapse) moments of elbows based on the experimental study at Commissariat à l'Energie Atomique (CEA), France:

$$M_0 = 0.715h^{2/3}(4R^2 t\sigma_y) \quad \text{(closing mode)} \tag{6}$$
$$M_0 = 0.722h^{1/3}(4R^2 t\sigma_y) \quad \text{(opening mode)} \tag{7}$$

All the above equations are applicable only for the pure in-plane bending moment. The effect of internal pressure is not taken into account. Goodall (1978b) was the first to propose the closed-form equation of limit load of elbows under combined internal pressure and in-plane bending moment through the small-displacement analysis. The equation proposed was

$$M_0 = 1.04h^{2/3}(1 - P_r R/2t\sigma_y)^{1/3}(D^2 t\sigma_y) \tag{8}$$

From the above equation it is seen that internal pressure (P_r) reduces the limit moment. This is against the observations of Rodabaugh (1979), Hilsenkopf et al. (1988), Touboul et al. (1989), Shalaby and Younan (1998a,b) and Chattopadhyay et al. (1999). This shortcoming of the equation is because of the small-displacement analysis by Goodall, which could not capture the stiffening effect of internal pressure. Touboul et al. (1989) proposed an equation for instability moment (maximum moment in the moment–rotation curve) under combined internal pressure and bending moment as follows:

$$M_0 = M_0(P_r = 0).\left[1 + \left(\frac{0.7}{h}\right).\left(\frac{P_r R}{t\sigma_y}\right)\right].\left[1.4 - 0.5\frac{P_r R}{t\sigma_y}\right] \tag{9}$$

where M_0 ($P_r = 0$) indicates the instability moment with no internal pressure. This equation did not differentiate between the opening and closing mode of bending moment whereas the effect of internal pressure on the limit moments are different for these two modes as observed by Shalaby and Younan (1998a,b), Chattopadhyay et al. (1999). Touboul et al. (1989), observed that the effect of pressure on plastic (collapse) moment is much less compared to the effect on plastic instability moment. However, no equation for plastic (collapse) moment under combined loading was proposed by Touboul et al. (1989). Recently Ayob et al. (2003) studied the interaction of internal pressure, in-plane moment and torque loadings on the 90° smooth piping elbows and long straight tangent pipes.

2.2. The present work

It is clear from the foregoing discussion that no plastic (collapse) moment equations are available for combined loading of internal pressure and bending moment. In the present work, elastic–plastic finite element analyses have been carried out to evaluate plastic (collapse) moments of un-cracked elbows subjected to combined internal pressure and in-plane bending moment. For various elbow factors and level of internal pressure, total 60 and 54 cases have been analyzed for closing and opening mode of bending moment respectively. Based on these results, two closed-form equations are proposed to evaluate the plastic (collapse) moments of elbows under combined internal pressure and in-plane closing and opening bending moment.

2.3. Finite element analysis

The finite element method is used to conduct the investigation of plastic (collapse) loads of elbows of various sizes under combined internal pressure and bending moment. General purpose finite element program NISA (1997) is used for this study. Non-linear finite element analysis has been carried out to determine the plastic (collapse) moments of elbow from moment–rotation curves for various geometric and loading combinations. Moment versus end rotation curves are generated through finite element analysis. Both geometric and material non-linearity have been considered in the analysis. Various aspects of finite element analysis are briefly mentioned below. More details may be found in Chattopadhyay et al. (2000) and Chattopadhyay (2002).

- Six long radius elbows ($R_b/R = 3$) with various wall thicknesses (t) have been analyzed, where R_b and R are the mean bend radius and mean radius of elbow cross section respectively. Table 1 shows the details. The elbow is connected with straight pipes of length equal to six times the mean cross sectional radius (Fig. 2).

Table 1
Geometry of the defect-free elbows considered in analysis to propose plastic (collapse) moment equations

R (mm)	t (mm)	R/t	R_b/R	$h = tR_b/R^2$
250	20	12.50	3	0.240
250	28	8.93	3	0.336
250	35	7.14	3	0.420
250	40	6.25	3	0.480
250	45	5.55	3	0.540
250	50	5.00	3	0.600

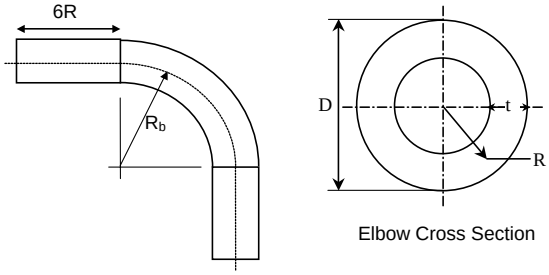

Fig. 2. Geometry of a 90° elbow.

Table 2
Material properties used in the analysis of defect-free elbows to propose plastic (collapse) moment equations

Yield stress (MPa)	270				
UTS (MPa)	513				
Young's modulus (GPa)	203				
Poisson's ratio	0.3				
True stress (MPa)	300	370	450	520	605
True strain	4.76×10^{-3}	0.0174	0.042	0.079	0.167

- The material is assumed isotropic. Strain hardening of the material is considered. Stress–strain response of a typical nuclear grade piping steel at room temperature has been considered in the analysis. Table 2 shows the material properties used in the analysis. Von-Mises yield criteria and isotropic hardening are assumed in the elastic–plastic analysis.
- The load in the elbows is split in two components: a constant internal pressure and varying in-plane bending moment monotonically increasing in steps. The various normalized pressures ($p = P_r R/t\sigma_y$) considered in the analysis are $p = 0$ (i.e. pure bending moment), 0.1157, 0.2314, 0.3471, 0.463, 0.5785, 0.6943, 0.8099, 0.9257 and 1.0. Closed end condition is simulated by applying axial pressure of intensity '$P_r R/2t$' at the end of the connecting straight pipe. Two modes of in-plane bending moment, namely, closing and opening are considered separately, as elbow deformations are distinctly different under these two different modes.
- Plastic (collapse) moment has been evaluated from the moment v/s end rotation curves by twice-elastic slope method, which is most consistent, reliable and reproducible and also recommended by ASME (2000).

2.4. Results and discussion

The effect of internal pressure on in-plane plastic (collapse) moment of defect-free elbows is investigated. Figs. 3 and 4 show the effect of normalized internal pressure on the normalized plastic (collapse) moments ($m_0 = M_0/(4R^2 t\sigma_y)$) of the elbows subjected to closing and opening mode of bending respectively. In both cases, it is observed that plastic (collapse) moment increases gradually with application of internal pressure. It reaches a peak and then starts falling with further increase in internal pressure. The beneficial effect of internal pressure is more pronounced for thin-walled elbows. This is in agreement with the observations of Shalaby and Younan (1998a,b). In case of opening mode, the basic nature of pressure effect is the same, but, the normalized plastic (collapse) moment starts dropping at lower values of normalized internal pressure.

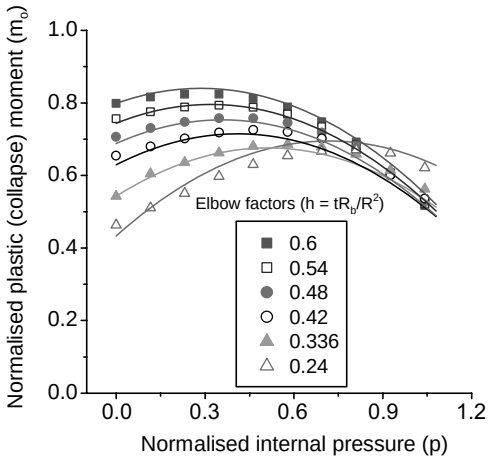

Fig. 3. Normalized closing plastic (collapse) moments for various normalized internal pressures and elbow factors (symbols show the FE results and solid lines show predictions of Eq. (10)).

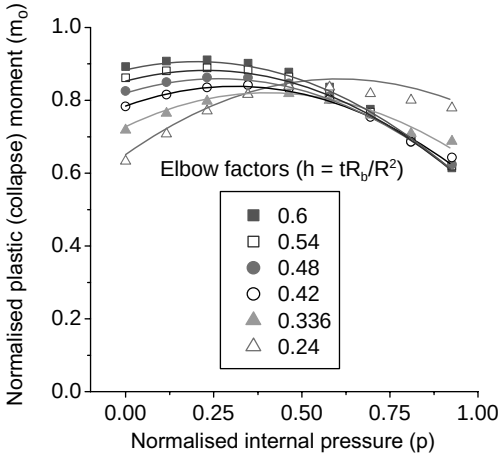

Fig. 4. Normalized opening plastic (collapse) moments for various normalized internal pressures and elbow factors (symbols show the FE results and solid lines show predictions of Eq. (11)).

2.5. Proposed equations

Based on the above results of the normalized limit moments for various sizes of defect-free elbows subjected to different levels of constant internal pressure and closing/opening in-plane bending moment, two equations are proposed to evaluate the plastic (collapse) moment:

$$m_0 = \frac{M_0}{4R^2 t\sigma_y} = 1.122h^{2/3} + 0.175\frac{p}{h} - 0.508p^2 \qquad \text{(for closing case)} \tag{10}$$

$$m_0 = \frac{M_0}{4R^2 t\sigma_y} = 1.047h^{1/3} + 0.124\frac{p}{h^{1.2}} - -0.568p^2 \quad \text{(for opening case)} \tag{11}$$

Applicability : $0.24 \leqslant h \leqslant 0.6$ and $0.0 \leqslant p \leqslant 1.0$

Figs. 3 and 4 show the comparison of fitted and finite element data. The fit seems to be quite satisfactory.

2.6. Checking the consistency of proposed equations

It is important to compare the present results with the results already available in the literature. The comparisons for un-pressurized and pressurized cases are done separately. For un-pressurized cases, Table 3 shows the comparison of normalized closing plastic (collapse) moment (m_0) for $h = 0.24$ and 0.42. It is seen that the present results are higher than those of Spence and Findlay (1973), Calladine (1974) and Touboul et al. (1989). This is due to two reasons—stiffening effect of connecting straight pipes and consideration of material strain hardening in the present analysis. This is comparable with the results of Griffiths (1979) who observed that 90° bend specimens without defects give consistently higher values of plastic (collapse) moments than those predicted by Calladine (1974) and this is predominantly due to the constraining effect of the connected pipes, an effect that becomes significant for $R_b/R < 3$. Griffiths (1979) suggests a factor of '1.33' to multiply the Calladine equation (Eq. (3)) to match his elbow test data for $R_b/R = 2$. From the present Eq. (10), the factor becomes 1.2 which is less than 1.33. This is understandable because the present analysis is for $R_b/R = 3$ and the stiffening effect reduces with increasing R_b/R.

For pressurized cases, the present results predicted by Eqs. (10) and (11) are compared with those predicted by Eq. (9) of Touboul et al. (1989) and digitized data from the graphs of Shalaby and Younan (1998a,b). The comparison is done in the form of $M_0(p)/M_0(p = 0)$ versus normalized internal pressure (p). Fig. 5 shows the comparison for a typical elbow factor, $h = 0.4132$. It may be noted that as per the present definition of elbow factor, $h = tR_b/R^2$, the elbow factor of 0.4417 in Shalaby and Younan (1998a,b) becomes 0.4132. It is seen from Fig. 5 that the effect of internal pressure on limit moment as per Touboul et al. (1989) is much more pronounced than that as per the present Eqs. (10) and (11). This

Table 3
Comparison of closing $m_0 = M_0/4R^2t\sigma_y$ for $p = 0.0$

h	Spence and Findlay (Eqs. (1) and (2))	Calladine (Eq. (3))	Touboul et al. (Eq. (6))	Griffiths (1.33 × Calladine)	Present (Eq. (10))
0.24	0.368	0.361	0.276	0.480	0.433
0.42	0.544	0.524	0.4	0.697	0.629

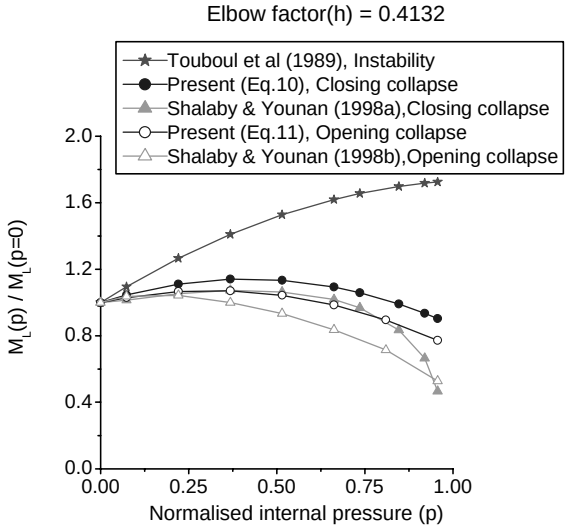

Fig. 5. Effect of internal pressure on limit moments—a comparison.

is expected since Eq. (9) of Touboul et al. (1989) is for instability moment and the present Eqs. (10) and (11) are for plastic (collapse) moments and Touboul et al. (1989) observed that the pressure effect is larger upon instability than upon collapse moments. The pressure effect on plastic (collapse) moments as per the present Eqs. (10) and (11) is consistently higher than those as per Shalaby and Younan (1998a,b). This is probably due to the consideration of material strain hardening in the present analysis as compared to the assumption of elastic–perfectly plastic material response by Shalaby and Younan. From the above discussion, it is concluded that the present results are consistent with the available test data and analytical results. Next stage of this work will be to investigate how plastic (collapse) moment will be affected if idealistic elastic–perfectly plastic material response is assumed in stead of realistic strain-hardening material.

3. New limit load equations of throughwall circumferentially cracked (TCC) elbow under in-plane bending moment

Pipe bends or elbows are commonly used components in a piping system. For safety analyses, especially for beyond-design loadings, it is very important to know the effect of cracks on the plastic (collapse) moments of elbows for integrity assessment of the piping system. Griffiths (1979) and Yahiaoui et al. (2002) observed that a throughwall circumferential crack in an elbow can significantly reduce its plastic (collapse) moment. Miller (1988) and Zahoor (1989–1991) gave closed-form expressions of plastic (collapse) moments of elbows with throughwall cracks based on Griffiths' experimental data (1979). Recently, Yahiaoui et al. (2002) while comparing their experimental results with theoretical predictions found that the existing solutions are excessively conservative and on occasions, non-applicable to the cases for which they are intended. Consequently, the present study has been undertaken to evaluate the plastic (collapse) load of throughwall circumferentially cracked (TCC) elbows subjected to in-plane opening/closing bending moments by elastic–plastic finite element analysis.

3.1. Methodology

Fig. 6a and b shows the geometry of a TCC elbow. The crack is centered at the extrados or the intrados depending on the mode of bending moment applied. The extrados crack is assumed for closing moment and the intrados crack is assumed for opening moment. A total of 72 cases of elbows with various sizes of circumferential cracks ($2\theta = 0$–$150°$), different wall thickness ($R/t = 5$–20), different elbow bend radii ($R_b/R = 2.3$) and two different bending modes, namely closing and opening have been considered in the analysis. Elastic-perfectly plastic stress–strain behavior of material has been assumed. Plastic (collapse) moments have been evaluated from moment–end rotation curves by twice-elastic slope method according to ASME (2000). Before analyzing cracked elbows, defect-free elbows have been analyzed for both closing and opening bending moments. Subsequently, the weakening factor because of the presence of crack has been quantified by evaluating the ratio of plastic (collapse) moments of cracked and defect-free elbows. From these results, new equations have been proposed to evaluate plastic (collapse) moments of elbows under closing and opening mode of bending moment. In this paper, mainly the results are discussed. More details are given in Chattopadhyay et al. (2004a,b).

3.2. Results of defect-free elbows

The plastic (collapse) moment equation of a defect-free elbow subjected to closing moment is, in general, given in the form:

$$M_0 = Ah^{2/3}(4R^2t\sigma_y) \quad (A \text{ is a constant}) \tag{12}$$

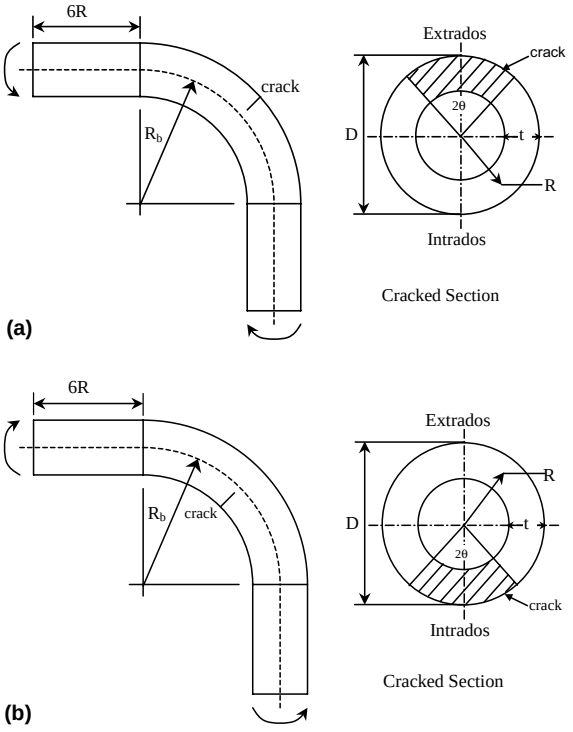

Fig. 6. Geometry of a throughwall circumferentially cracked elbow under (a) closing moment and (b) opening moment.

Fig. 7 shows the variation of normalized plastic (collapse) moment ($M_0/(4R^2t\sigma_y)$) with $h^{2/3}$ for the present analysis. A best-fit line is drawn and the constant 'A' is evaluated as 1.075. This is higher than 0.935 of Calladine (1974) because of constraining effect of connected straight pipes, smaller than 1.122 of Eq. (10) because strain-hardening is not considered in the present analysis and almost comparable with 1.04 by Goodall (1978a) who had done similar analysis.

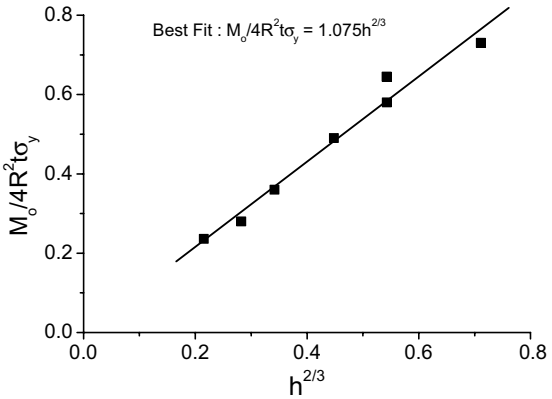

Fig. 7. Variation of normalized plastic (collapse) moment of deflect-free elbow under closing bending with elbow factor.

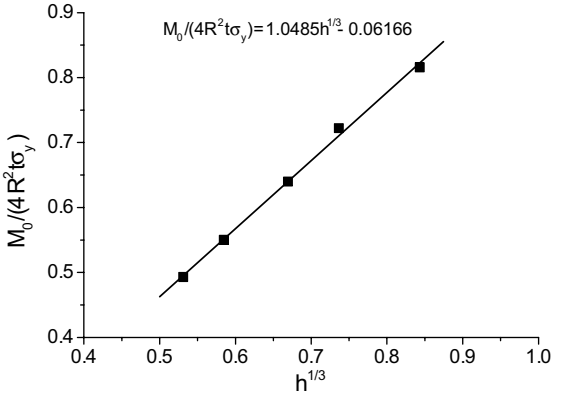

Fig. 8. Variation of normalized plastic (collapse) moment of deflect-free elbow under opening bending with elbow factor.

The plastic (collapse) moment equation of a defect-free elbow under opening moment is, in general, given in the form:

$$M_0 = Ch^{1/3}(4R^2t\sigma_y) \quad (C \text{ is a constant}) \tag{13}$$

where C has been proposed to be 0.722 by Touboul et al. (1989), 1.047 in Eq. (11) considering strain-hardening effect. Fig. 8 shows the variation of normalized plastic (collapse) moment ($M_0/(4R^2t\sigma_y)$) with $h^{1/3}$ for the present analysis. A best-fit line is drawn and the equation derived is as follows:

$$\frac{M_0}{4R^2t\sigma_y} = 1.0485h^{1/3} - 0.0617 \tag{14}$$

The plastic (collapse) moment predicted by this equation is slightly lower than that predicted by Eq. (11). This is because elastic–perfectly plastic material response has been assumed here whereas strain-hardening material response was assumed in Eq. (11).

3.3. Effect of crack on plastic (collapse) moment

3.3.1. Closing mode

Fig. 9 shows the effect of crack on the plastic (collapse) moment of TCC elbows subjected to closing bending moment. All the data points have been generated for long radius elbows ($R_b/R = 3$). The weakening factor due to the presence of crack, expressed as the ratio of plastic (collapse) moments of cracked elbows to that of the defect-free elbows (M_L/M_0) is plotted as a function of crack angle (2θ) and R/t. It may be seen that up to a certain crack angle, there is no weakening effect on the plastic (collapse) moment. In other words, there is a threshold crack angle beyond which it starts weakening the elbow. This threshold crack angle increases with increasing R/t. For example, it is seen from the present results in Fig. 9 that for $R/t = 5$, the threshold crack angle is $2\theta = 45°$ as against $2\theta = 90°$ for $R/t = 20$. The physical explanations and experimental validations for the presence of threshold crack angle are given in Chattopadhyay et al. (2004a,b, 2005a).

It may also be seen from Fig. 9 that the presence of a large circumferential crack in a thicker elbow ($R/t = 5$) is much more weakening than the presence of same size of crack in a thinner elbow ($R/t = 20$).

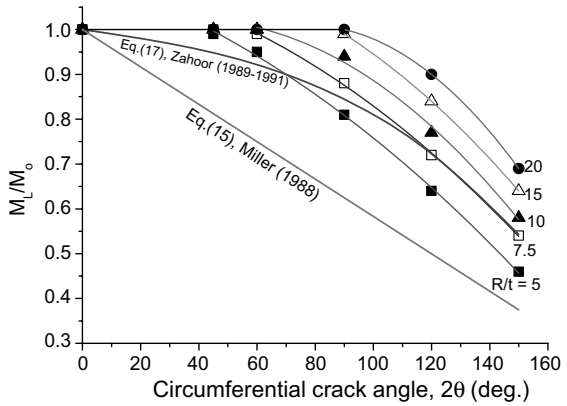

Fig. 9. Variation of normalized plastic (collapse) moment with crack angle for closing moment (symbols show the present FE results and solid lines show predictions of closed-form equations).

It is interesting to compare the present results with that of Miller (1988) and Zahoor (1989–1991). Miller (1988) proposed the following equation to evaluate plastic (collapse) moment (M_L):

$$\frac{M_L}{M_0} = 1 - \frac{3\theta}{2\pi} \tag{15}$$

$$M_0 = 0.935(4R^2 t\sigma_f)h^{2/3} \tag{16}$$

where 2θ is the total crack angle and 'σ_f' is the material flow stress usually taken as average of yield and ultimate strength.

The equation proposed by Zahoor (1989–1991) was as follows:

$$M_L = M_0\left[1 - 0.2137\left(\frac{a}{D_m}\right) - 0.0485\left(\frac{a}{D_m}\right)^2 - 1.0559\left(\frac{a}{D_m}\right)^3\right] \tag{17}$$

Applicability : $a/D_m \leqslant 0.8$, $h \leqslant 0.5$ and $D_m/t \geqslant 15$

where M_0 is as defined in Eq. (16), a is the half crack length, D_m is the mean diameter of the elbow cross section.

Eq. (17) of Zahoor (1989–1991) is valid for $R/t \geqslant 7.5$ and it is seen from Fig. 9 that Zahoor's equation envelopes all the results above $R/t \geqslant 7.5$ in a conservative way. But the degree of conservatism is high for thinner elbows. The predictions by Eq. (15) of Miller (1988) is seen to be very conservative.

3.3.2. Opening mode

Fig. 10 shows the effect of cracks on the plastic (collapse) moments of elbows subjected to opening bending. All the data points have been generated for long radius elbows ($R_b/R = 3$). Like closing mode, the weakening factor due to the presence of crack, expressed as M_L/M_0, is plotted as a function of crack angle (2θ) and R/t. It may be seen that the effect of 'R/t' on the weakening factor is much smaller compared to the closing mode of bending. It may also be seen that the weakening effect of crack is evident even for smaller crack angles. Unlike closing mode, there is no threshold crack angle below which weakening effect is absent. Again, the physical explanation for this has been given in Chattopadhyay et al. (2004b, 2005a). It is also seen from Figs. 9 and 10 that weakening effect of an intrados crack under opening bending moment is more than an extrados crack of same size under closing bending moment.

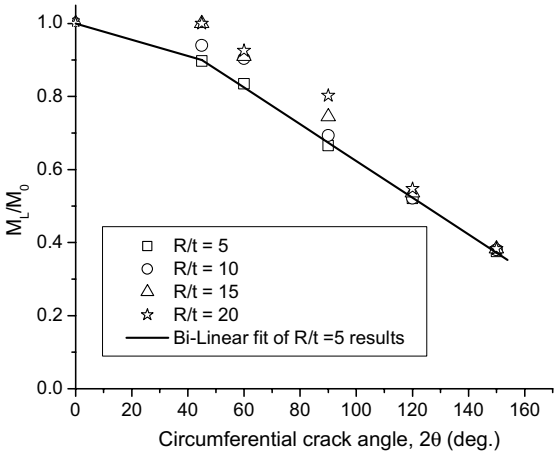

Fig. 10. Variation of normalized plastic (collapse) moment with crack angle for opening bending (symbols show the present FE results and solid lines show predictions of closed-form equations).

3.4. Effect of bend radius on weakening factor

Effect of bend radius on weakening factor due to crack has been investigated through comparison between few long ($R_b/R = 3$) and short ($R_b/R = 2$) radius elbows for various crack sizes, R/t ratios and bending mode. Fig. 11 shows the comparison of weakening factor, expressed as $X = M_L/M_0$ (defined earlier), for one typical closing case. It is seen that there is practically no effect of bend radius on the weakening factors.

3.5. Proposed plastic (collapse) moment equations

3.5.1. Closing mode

Figs. 7 and 9 show all the normalized plastic (collapse) moment data points obtained from non-linear finite element analysis for defect-free and cracked elbows subjected to closing mode of bending moment.

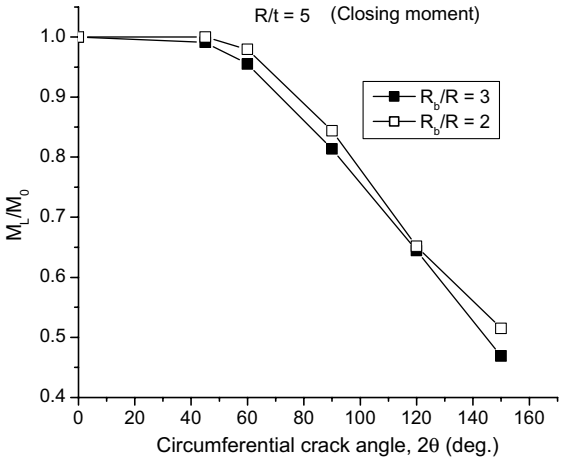

Fig. 11. Effect of bend radius on plastic (collapse) moment—a comparison for $R/t = 5$ and closing bending moment.

These data points have been best fitted to obtain closed-form plastic (collapse) moment equations. The basic form of the equation is as follows:

$$M_L = M_0 X \tag{18}$$

$$M_0 = 1.075 h^{2/3}(4R^2 t\sigma_y) \tag{19}$$

where M_L and M_0 are the plastic (collapse) moments of cracked and defect-free elbows respectively and X is the weakening factor, which is a function of crack size and R/t of the elbow. The functions to evaluate weakening factors for various R/t are given below. All these equations are valid for $0 \leqslant 2\theta \leqslant 150°$.

For $R/t = 5$

$$\begin{aligned} X &= 1.1194 - 0.7236\left(\frac{\theta}{\pi}\right) - 2.0806\left(\frac{\theta}{\pi}\right)^2 \quad \text{for } 45° \leqslant 2\theta \leqslant 150° \\ &= 1 \quad \text{for } 2\theta < 45° \end{aligned} \tag{20}$$

For $R/t = 7.5$

$$\begin{aligned} X &= 1.1185 - 0.342\left(\frac{\theta}{\pi}\right) - 2.52\left(\frac{\theta}{\pi}\right)^2 \quad \text{for } 60° \leqslant 2\theta \leqslant 150° \\ &= 1 \quad \text{for } 2\theta < 60° \end{aligned} \tag{21}$$

For $R/t = 10$

$$\begin{aligned} X &= 0.9655 + 1.0152\left(\frac{\theta}{\pi}\right) - 4.68\left(\frac{\theta}{\pi}\right)^2 \quad \text{for } 60° \leqslant 2\theta \leqslant 150° \\ &= 1 \quad \text{for } 2\theta < 60° \end{aligned} \tag{22}$$

For $R/t = 15$

$$\begin{aligned} X &= 1.14 + 0.3\left(\frac{\theta}{\pi}\right) - 3.6\left(\frac{\theta}{\pi}\right)^2 \quad \text{for } 90° \leqslant 2\theta \leqslant 150° \\ &= 1 \quad \text{for } 2\theta < 90° \end{aligned} \tag{23}$$

For $R/t = 20$

$$\begin{aligned} X &= 0.64 + 3.42\left(\frac{\theta}{\pi}\right) - 7.92\left(\frac{\theta}{\pi}\right)^2 \quad \text{for } 90° \leqslant 2\theta \leqslant 150° \\ &= 1 \quad \text{for } 2\theta < 90° \end{aligned} \tag{24}$$

Fig. 9 shows the predictions of these equations as solid lines. It may be seen that these equations fit almost exactly with the finite element data points. For intermediate R/t values, X can be linearly interpolated between the adjacent R/t values. However, for conservative results, the equation applicable for next lower R/t may be chosen.

3.5.2. Opening mode

Figs. 8 and 10 show all the normalized plastic (collapse) moment data points obtained from non-linear finite element analysis for defect-free and cracked elbows subjected to opening mode of bending moment. These data points have been best fitted to obtain plastic (collapse) moment equations. The basic form of the equation is as given in Eq. (18) with M_0 defined in Eq. (14). Since the weakening factor (X) because of the presence of crack does not strongly depend on R/t, it has been conservatively generated for $R/t = 5$ by bi-linear curve fitting and can be used for $5 \leqslant R/t \leqslant 20$. The equations proposed are as follows:

$$\begin{aligned} X &= 1.127 - 1.8108\left(\frac{\theta}{\pi}\right) \quad \text{for } 45^\circ \leqslant 2\theta \leqslant 150^\circ \\ &= 1 - 0.8\left(\frac{\theta}{\pi}\right) \qquad\quad \text{for } 0^\circ \leqslant 2\theta \leqslant 45^\circ \end{aligned} \tag{25}$$

4. New η_{pl} and γ functions for various cracked pipe and elbow geometry to evaluate J–R curve from test data

J–resistance (J–R) curve is one of the important material input parameters in the integrity assessment of cracked structures. Experimental evaluation of the J–R curve requires the 'η_{pl}' function (Rice et al., 1973) to multiply the area under the load vs. plastic load-line-displacement curve. However, J-integral, thus evaluated, requires modification if crack growth occurs. A 'γ' term was proposed by Hutchinson and Paris (1979) and later generalized by Ernst et al. (1979) and Ernst and Paris (1980) to correct the J-integral to account for the crack growth. The 'η_{pl}' and 'γ' functions are available for limited geometry under specified loading conditions (Hutchinson and Paris, 1979; Ernst et al., 1979; Ernst and Paris, 1980; Zahoor and Kanninen, 1981; Wilkowski et al., 1981; Ernst et al., 1981; Zahoor and Norris, 1984; Rajab and Zahoor, 1990; Zhou et al., 1991). These functions have been derived from dimensional analyses that are specific to the geometry and loading conditions. Roos et al. (1986) proposed limit load based general expression of 'η_{pl}' function. However, its application was restricted to small specimens. Recently, Chattopadhyay et al. (2001) derived limit load based general expressions of 'η_{pl}' and 'γ' functions. The advantage of these general expressions is that 'η_{pl}' and 'γ' functions can be very easily determined for any crack geometry, because limit load expressions of most of the cracked components of general interest are easily available in the literature (Miller, 1988; Zahoor, 1989–1991; Chattopadhyay et al., 2004a,b). Even if the limit load expression for particular crack geometry is not available in the literature, it can be determined from finite element analysis (see for example, Chattopadhyay et al., 2004a,b). However, there is no direct numerical/analytical method to evaluate the 'η_{pl}' and 'γ' functions for any cracked geometry. With this new method proposed by Chattopadhyay et al. (2001), it is possible to modify the existing 'η_{pl}' and 'γ' functions if a better limit load formula for particular crack geometry is available in future. The present paper uses the limit load based general expressions proposed in Chattopadhyay et al. (2001) to derive new 'η_{pl}' and 'γ' functions to evaluate J–R curve from pipes and elbows with various crack configurations under different loading conditions.

4.1. Background

The evaluation of J-integral from test data generally requires the experimental load vs. load-line displacement and load vs. crack growth data. Rice et al. (1973) proposed splitting the total J-integral into elastic (J_e) and plastic (J_p) components:

$$J = J_e + J_p \tag{26}$$

J_e is evaluated as

$$J_e = K^2/E' \tag{27}$$

where $E' = E$ for plane stress case and $E' = E/(1-\nu^2)$ for plane strain case, K is the elastic stress intensity factor, E is the Young's modulus and ν is the Poisson's ratio. The general expression to evaluate J_p from experimental data is as follows (Zahoor, 1989–1991; Rice et al., 1973; Ernst et al., 1979; Zahoor and Kanninen, 1981):

$$J_p = \int_0^{\Delta_{pl}} \eta_{pl} \cdot P \cdot d\Delta_{pl} + \int_{a_0}^{a} \gamma \cdot J_p \cdot da \tag{28}$$

where P is the total applied load, Δ_{pl} is the plastic load-line displacement due to crack only, a_0 is the initial crack length per crack tip, a is the current crack length per crack tip, η_{pl} and γ are two geometry and loading dependent functions.

Eq. (28) is solved iteratively. First, an approximate 'J_p' is evaluated using the first term on the right hand side (RHS) of Eq. (28). Subsequently, this approximate 'J_p' is corrected by the second term of the RHS of Eq. (28). Zahoor and Kanninen (1981) suggested that if a sufficiently small increment of crack growth (Δa) is chosen, convergence is achieved in the first iteration. The above process of iteration can be expressed as (Zahoor, 1989–1991):

$$J_p = J_{po} + \int_{a_0}^{a} \gamma \cdot J_{po} \cdot da \tag{29}$$

$$J_{po} = \int_{0}^{\Delta_{pl}} \eta_{pl} \cdot P \cdot d\Delta_{pl} \tag{30}$$

If the trapezoidal rule of numerical integration is invoked to solve Eqs. (29) and (30), 'J_p' can be expressed as follows:

$$J_{p_i} = [J_{p_{i-1}} + \eta_{pl_{i-1}} \cdot (U_{pl_i} - U_{pl_{i-1}})] \cdot [1 + \gamma_{i-1}(a_i - a_{i-1})] \tag{31}$$

with,

$$(U_{pl_i} - U_{pl_{i-1}}) = \left(\frac{P_{i-1} + P_i}{2}\right) \cdot (\Delta_{pl_i} - \Delta_{pl_{i-1}}) \tag{32}$$

where U_{pl} is the area under the load vs. plastic load-point-displacement curve. The subscripts 'i' and '$i-1$' indicate the current and previous load steps respectively. The load, P and plastic load-line displacement, Δ_{pl} are used here in a generic sense. For moment loading, applied load indicates the applied moment (M) and plastic load-line displacement indicates the plastic load-point rotation (ϕ_{pl}). It should also be noted that displacements for evaluation of J-integral by this approach are due to crack only. In other words, displacement of defect-free component should be subtracted from the total displacement to evaluate plastic J-integral. Although, it has been seen that for deeply cracked structure, the role of defect-free component displacement is almost insignificant.

Recently Chattopadhyay et al. (2001) derived the limit load-based general expressions of 'η_{pl}' and 'γ' functions as follows:

$$\eta_{pl} = -\frac{\partial F_L}{\partial A} \cdot \frac{1}{F_L} \tag{33}$$

$$\gamma = \frac{\partial^2 F_L / \partial a^2}{\partial F_L / \partial a} \tag{34}$$

These general expressions of 'η_{pl}' and 'γ' functions have been extensively validated analytically by deriving almost all the existing 'η_{pl}' and 'γ' functions of TPB specimens and pipes with various crack configurations under different loading conditions (Chattopadhyay et al., 2001). Even a typographical error in γ expression of throughwall circumferentially cracked pipe under axial tension in Zahoor (1989–1991) has been pointed out in Chattopadhyay et al. (2001). Utilizing these general expressions, new 'η_{pl}' and 'γ' functions for various cracked pipe/elbow geometry under various loading conditions, for which no solutions are available in the open literature, have been derived. They are shown in the following section. Details of these derivations and experimental/numerical validations of some of these new 'η_{pl}' and 'γ' functions are available in Chattopadhyay et al. (2004c,d).

4.2. New 'η_{pl}' and 'γ' functions

New 'η_{pl}' and 'γ' functions for the following geometries have been derived:

- throughwall circumferentially cracked thick pipe under combined bending and tension (Fig. 12);
- pipe with constant depth part-through circumferential crack under combined bending moment and axial tension (Fig. 13);
- pipe with semi-elliptical part-throughwall circumferential crack under axial tension (Fig. 14);
- pipe with semi-elliptical part-throughwall circumferential crack under combined bending moment and axial tension (Fig. 15);
- pipe with full circumferential part-throughwall crack under axial tension (Fig. 16);
- elbow with throughwall circumferential crack under in-plane bending moment (Fig. 6);
  - closing moment,
  - opening moment,
- elbow with throughwall axial crack under in-plane bending moment (Fig. 17);
  - long radius elbows,
    - crack at extrados,
    - crack at crown,
    - crack at intrados,

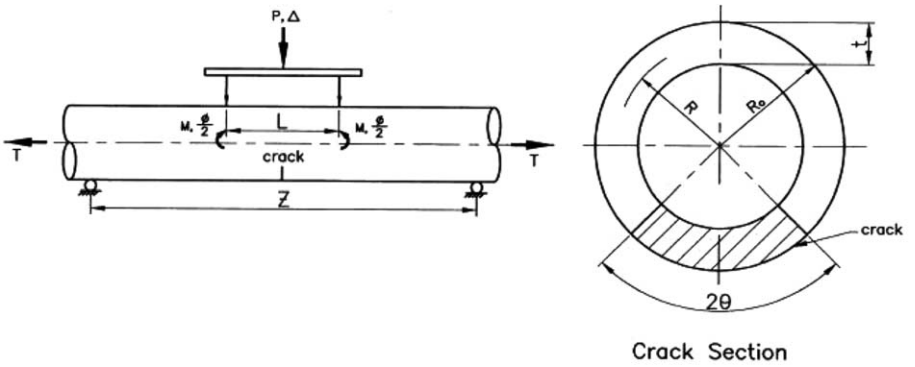

Fig. 12. Pipe with throughwall circumferential crack under combined bending and tension.

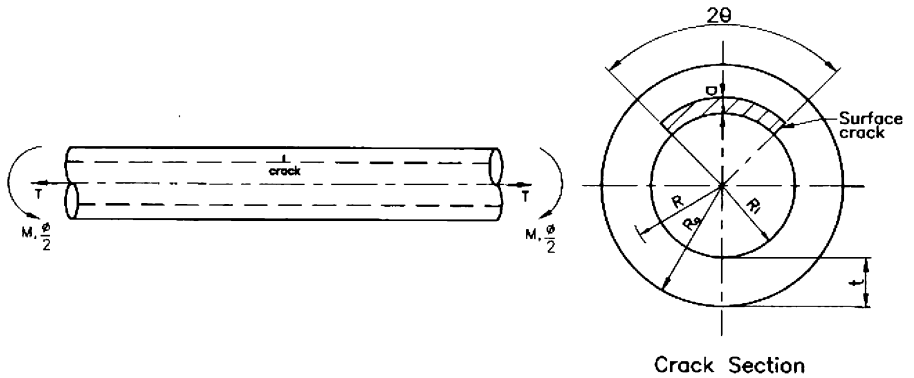

Fig. 13. Pipe with semi-elliptical surface crack under combined bending and tension.

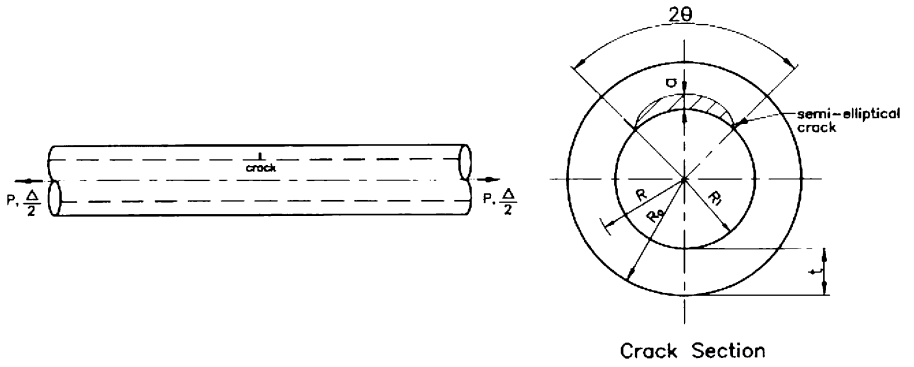

Fig. 14. Pipe with semi-elliptical surface crack under axial tension.

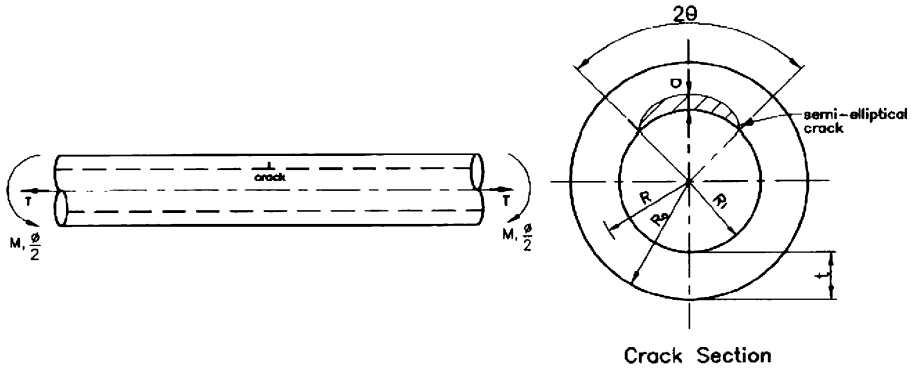

Fig. 15. Pipe with constant-depth part-through circumferential crack under combined tension and bending.

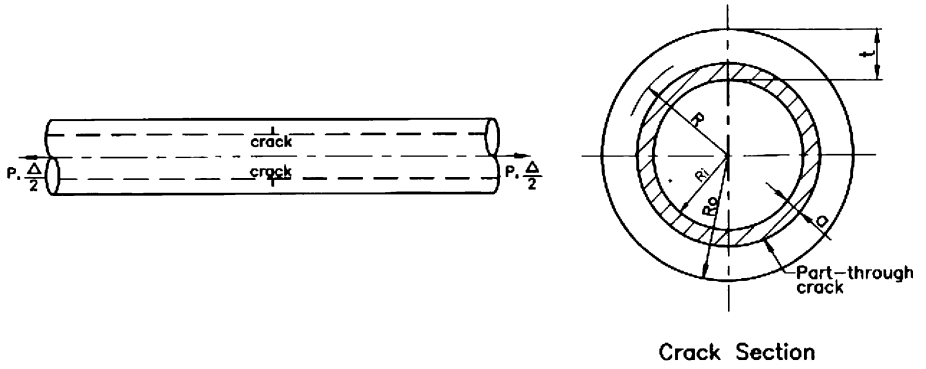

Fig. 16. Pipe with full circumferential part-through crack under axial tension.

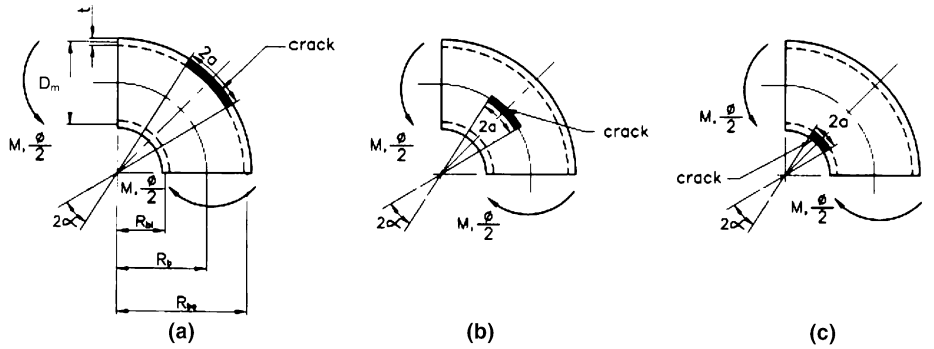

Fig. 17. Elbow with throughwall axial crack at (a) extrados, (b) crown and (c) intrados under in-plane bending moments.

– short radius elbows,
  * crack at extrados,
  * crack at crown,
  * crack at intrados.

Table 4 shows the new 'η_{pl}' and 'γ' functions. Eqs. (29)–(32) are to be used to evaluate J_p with these 'η_{pl}' and 'γ' functions and see the figures and nomenclature for meaning of symbols. It should be noted that for moment loading of an elbow as shown in Fig. 17(a), Eq. (30) is modified as

$$J_{po} = \int_0^{\phi_{pl}} \eta_{pl} \cdot M \cdot d\phi_{pl} \tag{35}$$

where 'ϕ_{pl}' is the plastic load-point rotation and 'M' is the applied moment.

5. Studying the effect of deformation on the unloading compliance

Unloading compliance technique is one of the convenient methods to measure crack growth during fracture experiments. However, one correlation expressing crack size as a function of unloading compliance is the pre-requisite of this technique. Such correlations are available (ASTM, 1999) for commonly used laboratory specimens, for example, compact tension (CT), three point bend (TPB) specimens, etc. Conventionally, compliance correlation is derived by generating compliance versus crack length data by performing small-displacement linear elastic finite element analysis. However, it does not account for the large deformation that may take place during the loading of the specimen. The unloading compliance may be influenced by the change in stiffness of the specimen because of change in basic geometry during large deformation. In that case, the compliance function not only depends on crack length but also on the current load/deformation. It is, therefore, of interest to study the effect, if any, of load/deformation on the unloading compliance. This requires carrying out non-linear finite element analysis to generate compliance data at different load levels. In the present work, investigation is carried out on three point bend (TPB) specimens and throughwall circumferentially cracked pipes under four point bending load.

5.1. Methodology

Each TPB (Fig. 18) and pipe (Fig. 19) specimen is loaded beyond limit load (P_L) with periodic unloading. The limit load/moment is computed using the following equations:

Table 4
New 'η_{pl}' and 'γ' functions for various pipe/elbow geometries

Sl. no.	Geometry	η_{pl} and γ
1	Pipe with TWCC[a] under axial tension plus bending (Fig. 12)	$\eta_{pl} = \frac{0.5[\sin\alpha' + \cos\theta]}{2Rt[\cos\alpha' - 0.5\sin\theta]}$, $\gamma = \frac{1}{R}\left(\frac{0.5\cos\alpha' - \sin\theta}{\sin\alpha' + \cos\theta}\right)$ with $\alpha' = 0.5\theta + \frac{T}{4\sigma_f R_0 t(1-\zeta)}$
2	Pipe with constant depth PTCC[b] under axial tension plus bending (Fig. 13)	$\eta_{pl} = \frac{1}{2R_i t}\frac{\left(\cos\beta + \frac{\sin\theta}{\theta}\right)}{(2\sin\beta - \frac{a}{t}.\sin\theta)}$, $\gamma = \frac{1}{2t}\frac{\sin\beta}{\left(\frac{\cos\beta}{\theta} + \frac{\sin\theta}{\theta^2}\right)}$ with $\beta = 0.5\pi[1 - (\frac{\theta}{\pi})\cdot(\frac{a}{t}) - s]$
3	Pipe with semi-elliptical PTCC[b] under axial tension (Fig. 14)	$\eta_{pl} = \left(\frac{2}{\pi^2 R_i t}\right)\frac{\left(1 + \frac{\sin\theta}{\theta\sin\psi}\right)}{\left(\frac{2\psi}{\pi} - \frac{x\theta}{\pi}\right)}$, $\gamma = \frac{\left(\frac{0.5}{t}\right)\left(\frac{\sin^2\theta}{\theta}\right)\left(\frac{\cot\psi}{\sin^2\psi}\right)}{\left(1 + \frac{\sin\theta}{\theta\sin\psi}\right)}$ with $\psi = \cos^{-1}(0.5x\sin\theta)$
4	Pipe with semi-elliptical PTCC[b] under axial tension plus bending (Fig. 15)	$\eta_{pl} = \frac{2}{\pi R_i t}\cdot\frac{\left(\cos\beta + \frac{\sin\theta}{\theta}\right)}{\left(2\sin\beta - \frac{a}{t}.\sin\theta\right)}$, $\gamma = \frac{1}{2t}\cdot\frac{\sin\beta}{\left(\frac{\cos\beta}{\theta} + \frac{\sin\theta}{\theta^2}\right)}$ with $\beta = 0.5\pi[1 - \left(\frac{\theta}{\pi}\right)\cdot\left(\frac{a}{t}\right) - s]$
5	Pipe with full circumferential PTCC[b] under axial tension (Fig. 16)	$\eta_{pl} = \frac{1}{2\pi Rt}\cdot\frac{\left(1 + \frac{a}{R_i}\right)}{\left(1 + \frac{a}{2R}\right)\cdot\left(1 - \frac{a}{t}\right)}$, $\gamma = \frac{1}{t\left(\frac{R_i}{t} + \frac{a}{t}\right)}$
6	(i) Elbow with TWCC[a] at extrados under closing moment ($R/t = 5$) (Fig. 6a)	$\eta_{pl} = \frac{1}{2Rt}\frac{(0.2303 + 0.4216\theta)}{(1.1194 - 0.2303\theta - 0.2108\theta^2)}$, $\gamma = \frac{1}{R}\frac{0.4216}{(0.2303 + 0.4216\theta)}$ $\theta/\pi \geqslant 0.125$
	(ii) Elbow with TWCC[a] at extrados under closing moment ($R/t = 7.5$)	$\eta_{pl} = \frac{1}{2Rt}\cdot\frac{(0.1089 + 0.5106\theta)}{(1.1185 - 0.1089\theta - 0.2553\theta^2)}$, $\gamma = \frac{1}{R}\cdot\frac{0.5106}{(0.1089 + 0.5106\theta)}$ $\theta/\pi \geqslant 0.167$
	(iii) Elbow with TWCC[a] at extrados under closing moment ($R/t = 10$)	$\eta_{pl} = \frac{1}{2Rt}\frac{(-0.3231 + 0.9484\theta)}{(0.9655 + 0.3231\theta - 0.4742\theta^2)}$, $\gamma = \frac{1}{R}\frac{0.9484}{(-0.3231 + 0.9484\theta)}$ $\theta/\pi \geqslant 0.167$
	(iv) Elbow with TWCC[a] at extrados under closing moment ($R/t = 15$)	$\eta_{pl} = \frac{1}{2Rt}\frac{(-0.0955 + 0.7294\theta)}{(1.14 + 0.0955\theta - 0.3647\theta^2)}$, $\gamma = \frac{1}{R}\frac{0.7294}{(-0.0955 + 0.7294\theta)}$ $\theta/\pi \geqslant 0.25$
	(v) Elbow with TWCC[a] at extrados under closing moment ($R/t = 20$)	$\eta_{pl} = \frac{1}{2Rt}\frac{(-1.0886 + 1.605\theta)}{(0.64 + 1.0886\theta - 0.8025\theta^2)}$, $\gamma = \frac{1}{R}\frac{1.605}{(-1.0886 + 1.605\theta)}$ $\theta/\pi \geqslant 0.25$

Table 4 (*continued*)

Sl. no.	Geometry	η_{pl} and γ
7	Elbow with TWCC[a] at intrados under opening moment ($5 \leqslant R/t \leqslant 20$), (Fig. 6b)	$\eta_{pl} = \frac{1}{2Rt}\frac{0.5764}{(1.127 - 0.5764\theta)}$ for $\theta/\pi \geqslant 0.125$ $\eta_{pl} = \frac{1}{2Rt}\frac{0.2546}{(1.0 - 0.2546\theta)}$ for $\theta/\pi < 0.125$ $\gamma = 0$
8	(i) Long radius elbow ($R_b/R = 3$) with TWAC[c] at extrados (Fig. 17a)	$\eta_{pl} = \frac{1}{2R_{bo}t}\cdot\frac{(0.4112 + 2.764\alpha - 4.1256\alpha^2)}{(1 - 0.4112\alpha - 1.382\alpha^2 + 1.3752\alpha^3)}$, $\gamma = \frac{1}{R_{bo}}\cdot\frac{(2.764 - 8.2512\alpha)}{(0.4112 + 2.764\alpha - 4.1256\alpha^2)}$
	(ii) Long radius elbow with TWAC[c] at crown (Fig. 17b)	$\eta_{pl} = \frac{1}{2R_bt}\frac{(0.1236 + 6.18975\alpha - 9.4435875\alpha^2)}{(1 - 0.1236\alpha - 3.094875\alpha^2 + 3.1478625\alpha^3)}$, $\gamma = \frac{1}{R_b}\frac{(6.18975 - 18.887175\alpha)}{(0.1236 + 6.18975\alpha - 9.4435875\alpha^2)}$
	(iii) Long radius elbow with TWAC[c] at intrados (Fig. 17c)	$\eta_{pl} = \frac{1}{2R_{bi}t}\frac{(0.0206 + 4.881\alpha - 6.7773\alpha^2 + 1.9264\alpha^3)}{(1 - 0.0206\alpha - 2.4405\alpha^2 + 2.2591\alpha^3 - 0.4816\alpha^4)}$, $\gamma = \frac{1}{R_{bi}}\frac{(4.881 - 13.5546\alpha + 5.7792\alpha^2)}{(0.0206 + 4.881\alpha - 6.7773\alpha^2 + 1.9264\alpha^3)}$
9	(i) Short radius elbow ($R_b/R = 2$) with TWAC[c] at extrados (Fig. 17a)	$\eta_{pl} = \frac{1}{2R_{bo}t}\cdot\frac{0.225}{(1 - 0.225\alpha)}$, $\gamma = 0$
	(ii) Short radius elbow with TWAC[c] at crown (Fig. 17b)	$\eta_{pl} = \frac{1}{2R_bt}\cdot\frac{0.15}{(1 - 0.15\alpha)}$, $\gamma = 0$
	(iii) Short radius elbow with TWAC[c] at intrados (Fig. 17c)	$\eta_{pl} = \frac{1}{2R_{bi}t}\cdot\frac{0.075}{(1 - 0.075\alpha)}$, $\gamma = 0$

[a] TWCC: Throughwall circumferential crack.
[b] PTCC: Part-through circumferential crack.
[c] TWAC: Throughwall axial crack.

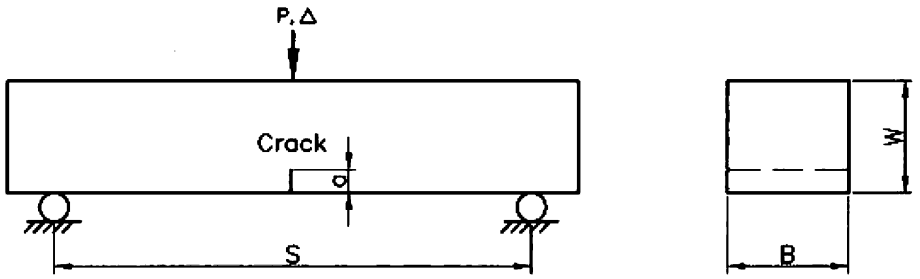

Fig. 18. ASTM SE(B) or TPB specimen.

$$\text{(For TPB specimen)} \qquad P_L = \frac{1.456b^2\sigma_f}{S} \tag{36}$$

$$\text{(For pipe)} \qquad M_L = 4R^2t\sigma_f\left[\cos\left(\frac{\theta}{2}\right) - 0.5\sin(\theta)\right] \tag{37}$$

where b is the remaining ligament in crack section and S is the loading span of TPB specimen, R is the mean radius of the pipe cross section, t is the pipe wall thickness, θ is the semi-circumferential crack angle, and σ_f is the material flow stress.

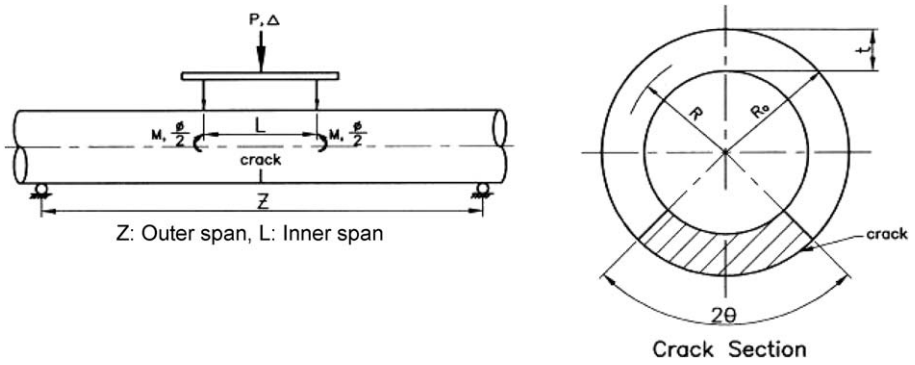

Fig. 19. Pipe with throughwall circumferential crack under four point bending load.

The load versus crack opening displacement has been generated for the entire load range with periodic unloading at 40%, 50%, 60%, 70%, 80%, 85%, 90%, 95%, 100%, 110%, 120%, 130%, 140%, 150%, 160% and 170% of limit load . The amount of unloading is 15% of limit load. Stiffness is evaluated from the slope of the load–CMOD curve by least square linear curve fitting of the unloading path. Compliance is evaluated by taking reciprocal of the stiffness at different stages of unloading including initial elastic portion. Compliance is defined as follows:

$$C = \frac{\delta}{P} \text{ (for TPB specimen)} \quad \text{and} \quad C = \frac{\delta}{M} \text{ (for pipe)} \tag{38}$$

where δ is the crack mouth opening displacement , P is the total load, M is the applied moment expressed as $M = P(Z - L)/4$ with Z, L as shown in Fig. 19.

Compliances are normalized as follows:

$$\text{(For TPB specimen (Kapp etal., 1985))} \qquad \lambda = \frac{1}{1 + \left(\frac{3.95S(1-\nu^2)}{\text{CEBw}}\right)^{0.5}} \tag{39}$$

$$\text{(For pipe)} \qquad \lambda = \text{CEI}/\pi R^2 \tag{40}$$

where λ is the normalized compliance, C is the compliance as defined in Eq. (38), E is the young's modulus and ν is the Poisson's ratio of material, I is the area moment of inertia of the pipe cross section and other symbols are explained in Figs. 18 and 19.

For TPB specimens, closed-form solution exists (Kapp et al., 1985) between the crack length and initial elastic compliance. The equation is as follows:

$$a/w = \lambda(-1.03 + 6\lambda - 6.37\lambda^2 + 2.73\lambda^3 - 0.312\lambda^4) \tag{41}$$

The present results have been validated against the above equation. Further, non-linear analysis has been performed to study how large deformation affects the above relation.

TPB specimens (Fig. 18) with different a/w ratios (0.1, 0.2, 0.3, 0.4, 0.5, 0.6, 0.7, 0.8 and 0.9) are considered in this analysis. Specimens have width (w) of 25 mm and unity thickness. The absolute value of specimen thickness does not play a role, because the compliance is normalized with respect to the thickness. The load span (S) is taken as four times of the width i.e. 100 mm.

In case of pipe, total six cases with different R/t ratios are considered to study the effect of R/t on normalized compliance. Table 5 shows the various combinations of outer diameter and thickness considered in this analysis. The inner and outer span of the four point bending load for 200 mm nominal bore (NB)

Table 5
Geometric details of straight pipes considered in the analysis to study the effect of deformation on unloading compliance

Outer diameter(mm)	Thickness (mm)	R/t
406	32.00	5.87
219	15.10	6.75
219	11.53	9.00
219	10.40	10.00
219	7.07	15.00
219	5.34	20.00

diameter pipe are 1480 and 4000 mm respectively and those for the 400 mm NB pipes are 1480 and 6000 mm respectively. Six throughwall circumferential crack angles, namely, 30°, 60°, 90°, 120°, 150° and 180° are considered for each size of pipe.

5.2. Results and discussion

5.2.1. TPB specimens

Fig. 20 shows the load vs. CMOD curves for all the specimens. Table 6 shows the actual a/w ratio and computed a/w ratio. The a/w for each specimen is calculated using Eq. (41) from normalized initial elastic

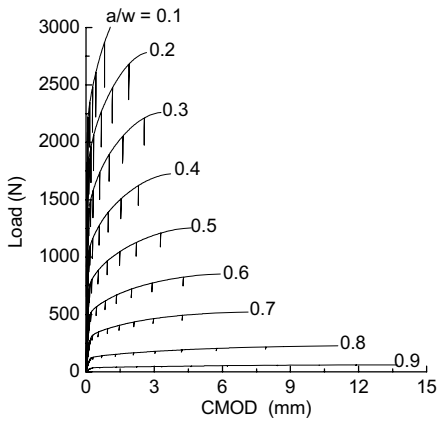

Fig. 20. Load vs. CMOD curves for TPB specimens with various a/w ratios.

Table 6
Comparison of a/w ratios using compliance method for TPB specimens

Actual a/w	Initial elastic compliance (C)	Normalized compliance, λ (Eq. (39))	Calculated a/w from Eq. (41)
0.1	0.13694E−04	0.30540	0.08653
0.2	0.30871E−04	0.39766	0.20380
0.3	0.54477E−04	0.46723	0.30200
0.4	0.91225E−04	0.53159	0.39584
0.5	0.15434E−03	0.59615	0.49005
0.6	0.27560E−03	0.66359	0.58644
0.7	0.54864E−03	0.73567	0.68570
0.8	0.13531E−02	0.81381	0.78820
0.9	0.56445E−02	0.89926	0.89528

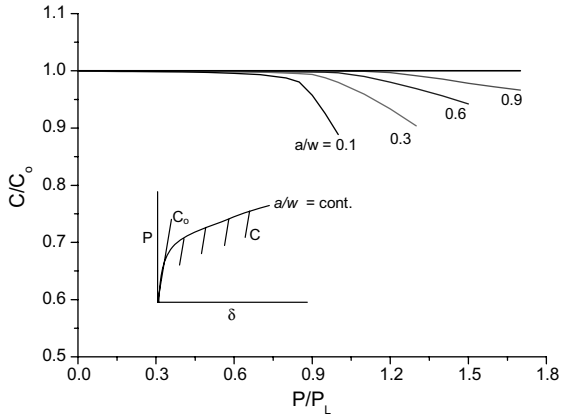

Fig. 21. Load/deformation effect on unloading compliance of TPB specimens with various a/w.

Table 7
Variation of normalized compliances, λ (Eq. (40)) with normalized load ($m = M/M_0$) for 200 and 400 mm NB pipes

m	$2\theta = 30°$	$2\theta = 60°$	$2\theta = 90°$	$2\theta = 120°$	$2\theta = 150°$	$2\theta = 180°$
$R/t = 5.84$ (400 mm NB pipe)						
0.0	0.3717	0.9287	1.8407	3.3587	5.9570	10.6645
0.8	0.4141	0.9147	1.8142	3.3035	5.8415	10.4355
1.0	0.3186	0.8593	1.7553	3.2296	5.7285	10.2430
1.2	–	0.7341	1.5971	3.0230	5.4295	9.7450
1.4	–	0.5560	1.4273	2.7924	5.1130	9.1600
1.6	–	–	1.2227	2.5503	4.7380	8.6160
1.7	–	–	0.9781	2.4293	4.5655	8.3710
1.8	–	–	–	2.2970	4.4018	8.1125
1.9	–	–	–	2.1446	4.2373	7.8655
2.0	–	–	–	1.9338	4.0685	7.6290
$R/t = 6.75$ (200 mm NB pipe)						
0.0	0.3601	0.9203	1.8555	3.4326	6.1425	11.0430
0.8	0.3541	0.9083	1.8307	3.3761	6.0181	10.7920
1.0	0.3175	0.8597	1.7774	3.3054	5.9040	10.5930
1.2	0.2511	0.7412	1.6237	3.1045	5.6120	10.1015
1.4	–	0.5869	1.4462	2.8614	5.2645	9.4815
1.6	–	–	1.2224	2.5973	4.8740	8.8960
1.7	–	–	1.0279	2.4583	4.6898	8.6050
1.8	–	–	–	2.3115	4.5058	8.3290
1.9	–	–	–	2.1399	4.3253	8.0645
2.0	–	–	–	1.8662	4.1393	7.8085
$R/t = 20$ (200 mm NB pipe)						
0.0	0.46929	1.47908	3.22230	6.08844	10.75080	18.68080
0.8	0.45058	1.41880	3.05264	5.68628	9.90097	17.22753
1.0	0.36769	1.30022	2.91264	5.47533	9.49553	16.46781
1.2	–	–	2.52440	5.00297	8.82544	15.23833
1.4	–	–	–	4.40767	8.11259	13.99478
1.6	–	–	–	–	–	12.89377
1.7	–	–	–	–	–	12.41831
1.8	–	–	–	–	–	11.98114
1.9	–	–	–	–	–	11.44143

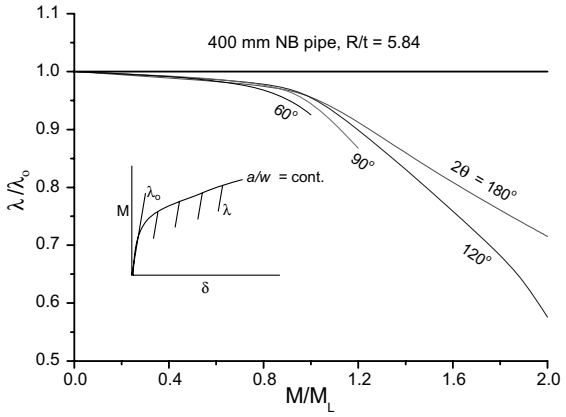

Fig. 22. Load/deformation effect on unloading compliance of pipes with various crack angles.

compliance to compare with actual a/w ratio and it is found that they are closely matching. It provides confidence in the present analysis. All specimens are not loaded to the same load level in times of limit load because of convergence problem. Except for one specimen with a/w ratio 0.1, all other are loaded beyond limit load. The maximum load level i.e. 170% of limit load is reached for the specimen with $a/w = 0.9$. Fig. 21 shows the ratio of initial elastic compliance (C_0) to the compliance values (C) at various load/deformation, quantified by (P/P_L). If there is no effect of load/deformation on unloading compliance, then C/C_0 should ideally be unity for constant crack length (a/w). It is seen that the C/C_0 is not really unity throughout, but the deviation from unity is much insignificant, specially for deeply cracked ($a/w > 0.5$) specimens, which are normally recommended by ASTM (1999). Therefore, the existing compliance correlation for TPB specimens based on linear elastic analysis does not require any modification to take care of geometric deformation at various load levels.

5.2.2. Straight pipes

Table 7 shows the normalized compliances, λ (see Eq. (40)) for 200 and 400 mm NB pipes with various sizes of cracks at various normalized load levels ($m = M/M_L$). It can be seen that unloading compliance decreases with increase in load even for the same crack length. This is because of ovalisation of the circular cross section of pipe during deformation. The pattern of ovalisation is such that it increases the area moment of inertia of pipe cross section, which is proportional to the fourth power of pipe diameter and hence stiffens the pipe under bending. Fig. 22 shows the ratio of initial elastic normalized compliance (λ_0) to the normalized compliance values (λ) at various load/deformation, quantified by (M/M_L). In contrast to TPB specimen (Fig. 21), it is seen from Fig. 22 that λ/λ_0 deviates significantly from unity indicating a strong influence of deformation on unloading compliance. It can also be seen that normalized compliances, λ for 200 and 400 mm NB pipes of almost same R/t ratios are almost identical at same normalized load level and normalized crack size (θ/π). However these values vary for pipes with different R/t ratio. Therefore, any compliance correlation of pipe must include load/deformation and R/t as the parameters.

6. Conclusions

Theoretical investigations of a comprehensive *Component Integrity Test Program* are described in this paper. As a result of these investigations, new plastic (collapse) moment equations of defect-free elbow

under combined internal pressure and in-plane closing/opening moments have been proposed; new plastic (collapse) moment equations of throughwall circumferentially cracked elbow are proposed, which are more accurate and closer to the test results; new 'η_{pl}' and 'γ' functions of pipes and elbows with various crack configurations under different loading conditions have been derived to evaluate the J–R curve from test data; and the effect of deformation on the unloading compliance of TPB specimen and throughwall circumferentially cracked pipe to measure crack growth during fracture experiment has also been done.

References

ASME Boiler and Pressure Vessel Code, 2000. Sec. III, American Society of Mechanical Engineers.

ASTM 1820-99, 1999. Standard test method for J-integral characterization of fracture toughness. American Society for Testing and Materials, Philadelphia.

Ayob, A.B., Moffat, D.G., Mistry, J., 2003. The interaction of pressure, in-plane moment and torque loadings on piping elbows. Int. J. Press. Vess. Piping 80, 861–869.

Calladine, C.R., 1974. Limit analysis of curved tubes. J. Mech. Eng. Sci., Inst. Mech. Eng. 16 (2), 85–87.

Chattopadhyay, J., 2002. The effect of internal pressure on in-plane collapse moment of elbows. Nucl. Eng. Des. 212 (March), 133–144.

Chattopadhyay, J., Venkatramana, W., Dutta, B.K., Kushwaha, H.S., 1999. Limit load of elbows under combined internal pressure and bending moment. In: Proceedings of the 15th International Conference on Structural Mechanics in Reactor Technology, SMiRT, Korea, vol. V, pp. 281–288.

Chattopadhyay, J., Nathani, D.K., Dutta, B.K., Kushwaha, H.S., 2000. Closed-form collapse moment equations of elbows under combined internal pressure and in-plane bending moment. J. Press. Vess. Technol., Trans. ASME 122, 431–436.

Chattopadhyay, J., Dutta, B.K., Kushwaha, H.S., 2001. Derivation of 'γ' parameter from limit load expressions of cracked component to evaluate J–R curve. Int. J. Press. Vess. Piping 78, 401–427.

Chattopadhyay, J., Tomar, A.K.S., Dutta, B.K., Kushwaha, H.S., 2004a. Closed form collapse moment equation of throughwall circumferentially cracked elbows subjected to in-plane bending moment. J. Press. Vess. Technol., ASME Trans. 126, 307–317.

Chattopadhyay, J., Tomar, A.K.S., Dutta, B.K., Kushwaha, H.S., 2004b. Limit load of throughwall cracked elbows: comparison of test results with theoretical predictions. Fatigue Fract. Eng. Mater. Struct. 27, 1091–1103.

Chattopadhyay, J., Dutta, B.K., Kushwaha, H.S., 2004c. New 'η_{pl}' and 'γ' functions to evaluate J–R curves from cracked pipes and elbows: part I—theoretical derivation. Eng. Fract. Mech. 71, 2635–2660.

Chattopadhyay, J., Dutta, B.K., Kushwaha, H.S., 2004d. New 'η_{pl}' and 'γ' functions to evaluate J–R curves from cracked pipes and elbows: part II—experimental and numerical validation. Eng. Fract. Mech. 71, 2661–2675.

Chattopadhyay, J., Pavankumar, T.V., Dutta, B.K., Kushwaha, H.S., 2005a. Fracture experiments on throughwall cracked elbows under in-plane bending moment: test results and theoretical/numerical analyses. Eng. Fract. Mech. 72, 1461–1497.

Chattopadhyay, J., Kushwaha, H.S., Roos, E., 2005b. Some recent developments on integrity assessment of pipes and elbows. Part II: Experimental investigations. Int. J. Solids Struct., in press, doi:10.1016/j.ijsolstr.2005.06.055.

Ernst, H.A., Paris, P.C., 1980. Techniques of analysis of load–displacement records by J-integral methods. NUREG/CR-1222, US Nuclear Regulatory Commission.

Ernst, H.A., Paris, P.C., Rossow, M., Hutchinson, J.W., 1979. Analysis of load displacement relation to determine J–R curve and tearing instability material properties. In: Smith, C.W. (Ed.), Fracture Mechanics, ASTM STP 677. American Society for Testing and Materials, Philadelphia, pp. 581–599.

Ernst, H.A., Paris, P.C., Landes, J.D., 1981. Estimations of J-integral and tearing modulus T from a single specimen test record. In: Roberts, R. (Ed.), Fracture Mechanics: Thirteenth Conference, ASTM STP 743. American Society for Testing and Materials, Philadelphia, pp. 476–502.

Gerdeen, J.C., 1979. A critical evaluation of plastic behavior data and a united definition of plastic loads for pressure components. Weld. Res. Counc. Bull., 254.

Goodall, I.W., 1978a. Large deformations in plastically deforming curved tubes subjected to in-plane bending. Research Division Report RD/B/N4312, Central Electricity Generating Board, UK.

Goodall, I.W., 1978b. Lower bound limit analysis of curved tubes loaded by combined internal pressure and in-plane bending moment. Research Division Report RD/B/N4360, Central Electricity Generating Board, UK.

Griffiths, J.E., 1979. The effect of cracks on the limit load of pipe bends under in-plane bending: experimental study. Int. J. Mech. Sci. 21, 119–130.

Hilsenkopf, P., Boneh, B., Sollogoub, P., 1988. Experimental study of behaviour and functional capability of ferritic steel elbows and austenitic stainless steel thin-walled elbows. Int. J. Pres. Ves. Piping 33 (2), 111–128.

Hutchinson, J.W., Paris, P.C., 1979. Stability analysis of *J*-controlled crack growth. In: Elastic–Plastic FractureASTM STP 668. American Society for Testing and Materials, Philadelphia, pp. 37–64.

Kapp, J.A., Leger, G.S., Gross, B., 1985. Wide range displacement expressions for standard fracture mechanics specimens. In: Kanninen, M.F., Hopper, A.T. (Eds.), Fracture Mechanics: Sixteenth Symposium, ASTM STP 868. American Society for Testing and Materials, Philadelphia, pp. 27–44.

Marcal, P.V., 1967. Elastic–plastic behavior of pipe bends with in-plane bending. J. Strain Anal. 2 (1), 84–90.

Miller, A.G., 1988. Review of limit loads of structures containing defects. Int. J. Press. Vess. Piping 32, 197–327.

NISA, 1997. A general purpose finite element program, Windows NT/95 Production Version, Engineering Mechanics Research Corporation, Michigan, USA.

Rajab, M.D., Zahoor, A., 1990. Fracture analysis of pipes containing full circumferential internal part-through flaw. Int. J. Press. Vess. Piping 41, 11–23.

Rice, J.R., Paris, P.C., Merkle, J.G., 1973. Some further results of *J*-integral analysis and estimates. In: Progress in Flaw Growth and Fracture Toughness TestingASTM STP 536. American Society for Testing and Materials, Philadelphia, pp. 231–245.

Rodabaugh, E.C., 1979. Interpretive report on limit load analysis and plastic deformations of piping products. Weld. Res. Counc. Bull. (254), 65–82.

Roos, E., Eisele, U., Silcher, H., 1986. A procedure for the experimental assessment of the *J*-integral by means of specimens of different geometries. Int. J. Press. Vess. Piping 23, 81–93.

Shalaby, M.A., Younan, M.Y.A., 1998a. Limit loads for pipe elbows with internal pressure under in-plane closing bending moment. J. Press. Vess. Technol., Trans. ASME 120 (1), 35–42.

Shalaby, M.A., Younan, M.Y.A., 1998b. Limit loads for pipe elbows subjected to in-plane opening moment and internal pressure. Paper Presented at the 1998 ASME/JSME Joint Pressure Vessels and Piping Conference held at San Diego, California, July 26–30, 1998, PVP-Vol. 368, pp. 163–170.

Spence, J., Findlay, G.E., 1973. Limit load for pipe bends under in-plane bending. In: Proceedings of the 2nd International Conference on Pressure Vessel Technology, San Antonio, 1–28, pp. 393–399.

Touboul, F., Ben Djedidia, M., Acker, D., 1989. Design criteria for piping components against plastic collapse: application to pipe bend experiments. In: Cengdian, L., Nichols, R.W. (Eds.), Pressure Vessel Technology, Proceedings of 6th International Conference Held in Beijing, 11–15th September 1988, pp. 73–84.

Wilkowski, G.M., Zahoor, A., Kanninen, M.F., 1981. A plastic fracture mechanics prediction of fracture instability in a circumferentially cracked pipe in bending—part II: experimental verification on a type 304 stainless steel pipe. J. Press. Vess. Technol., Trans. ASME 103, 359–365.

Yahiaoui, K., Moreton, D.N., Moffat, D.G., 2002. Evaluation of limit load data for cracked pipe bends under opening bending and comparisons with existing solutions. Int. J. Pres. Ves. Piping 79, 27–36.

Zahoor, A., 1989–1991. Ductile Fracture Handbook, vol. 1–3, EPRI-NP-6301-D, N14-1, Research Project 1757-69, Electric Power Research Institute.

Zahoor, A., Kanninen, M.F., 1981. A plastic fracture mechanics prediction of fracture instability in a circumferentially cracked pipe in bending—part I: *J*-integral analysis. J. Press. Vess. Technol., Trans. ASME 103, 352–358.

Zahoor, A., Norris, D.M., 1984. Ductile fracture of circumferentially cracked type 304 stainless steel pipes in tension. J. Press. Vess. Technol., Trans. ASME 106, 399–404.

Zhou, Z., Lee, K., Herrera, R., Landes, J.D., 1991. Normalisation: an experimental method for developing *J–R* curve. In: Joyce, J.A. (Ed.), Elastic–Plastic Fracture Test Methods: The User's Experience (Second Volume), ASTM STP 1114. American Society for Testing and Materials, Philadelphia, pp. 42–56.